Synthesis, photophysics, and theoretical calculations of styryl-based fluorophores harboring substituted benzothiazole acceptors

Mauro Safir Filho,[a,*] Emmanuel Santos Moraes,[b] Lilian Camargo da Luz,[c] Fabiano da Silveira Santos,[c] Anthony R. Martin,[a,d] Rachid Benhida,[a,e] Luís Gustavo Teixeira Alves Duarte,[b] Fabiano Severo Rodembusch[c,*]

[a]Institut de Chimie de Nice CRNS UMR7272, Université Côte d'Azur, 28 Avenue Valrose 06108 Nice, France. Email: mauro.safir-filho@univ-cotedazur.fr
[b]Chemistry Institute, University of Campinas, Campinas, 13083-970, Brazil.
[c]Grupo de Pesquisa em Fotoquímica Orgânica Aplicada. Instituto de Química (UFRGS), Av. Bento Gonçalves, 9500, CEP 91501-970. Porto Alegre-RS, Brazil. Email: rodembusch@iq.ufrg.br
[d]Institut des Biomolécules Max Mousseron, IBMM, Univ. Montpellier, ENSCM, CNRS, Montpellier, France
[e]Mohamed VI Polytechnic University, UM6P, 43150, Ben Guerir, Morocco

*Corresponding authors

Abstract

This study describes the synthesis, photophysical characterization, and TD-DFT calculation of a series of benzothiazole-based styryl fluorophores (**F1**-**F5**) harboring a D-π-A structure. The compounds were obtained through a simple and efficient synthetic route using low-cost starting materials. The investigation and analysis of their photophysical properties enable the assessment of the effect of four substituted benzothiazole moieties (A) and two types of π-conjugated frameworks (phenyl *vs* thienyl) in solution and in solid state. The fluorophores disclose absorption in the ultraviolet-blue region with a moderate solvatochromic effect and a single emission band located at the blue-green spectral range. In the solid state, the fluorophores showed emission in the green-orange regions with a relatively large Stokes shift. The systematic UV-Vis solvatochromism study and theoretical predictions using the CPCM model reveals the increment in the dipole moment of the systems in an excited state with the solvent dielectric constant. These compounds showed high

fluorescence quantum yield in solution and in solid-state and could be further exploited for solid-state lighting devices, or embedded in the design of biological dyes.

Keywords: solvatochromism; benzothiazole; large Stokes shift; push-pull; solvent effect; theoretical calculations.

1. Introduction

Fluorescent dyes featuring push-pull arrangements have gained notable attention in recent years. Among the different fluorescent dye families, neutral and positively charged styryl fluorophores have been subjected to an intensive investigation for a wide range of optical applications including ion sensing [1], molecular probes and markers [2], bioimaging [3-5], and optoelectronic devices [6,7]. Structurally, styryl-like push-pull fluorophores encompass a large class of molecules featuring electron-donating (D) and electron-acceptor (A) groups tethered by a vinyl linkage (D-π-A) [8]. Not surprisingly, this molecular arrangement allows dipolar structures at the ground or excited states that may generate specific luminescent outputs in response to a stimulus like light [9], polarity [8], hydration/solvation [6], viscosity [10], confinement [11], or electric field modifications [12]. In particular, the relaxation of the excited fluorophore through specific mechanisms, such as charge transfer [8,10], excited-state intramolecular proton transfer [13], and redox process [7], for example, in response to the aforementioned environmental changes, renders the D-π-A styryl fluorophores a valuable alternative to project high-performance molecular probes and active materials for different applications.

In our laboratories, we recently described and expanded the use of heterocyclic building blocks based on 6-aminosubstituted benzothiazole platforms and developed new sets of environment responsive and/or solvatofluorochromic styryl fluorophores [8]. We have demonstrated that these families of benzothiazole-based styryl fluorophores (Figure 1) combine excellent biocompatibility with easily modulated spectroscopic properties, thus making them a versatile fluorescent toolbox *per se*. Of note, the successful conversion of these fluorophores into molecular probes designed for particular biological applications was also assigned in our group, by employing smooth and

straightforward chemical transformations [14-16]. Thus, in line with the aforementioned background, we aim to expand our understanding of these groups of fluorophores. Herein, we envisioned the investigation of novel benzothiazole-based styryl analogs featuring a reverse D-π-A arrangement, *i.e.*, the anchoring of the electron-donating amino group at the opposite side of the benzothiazole framework (Figure 1). It is noteworthy that this alternative arrangement may confer new photophysical properties compared with the former fluorophores by reorienting the fluorophore dipole moment along the π-conjugated backbone.

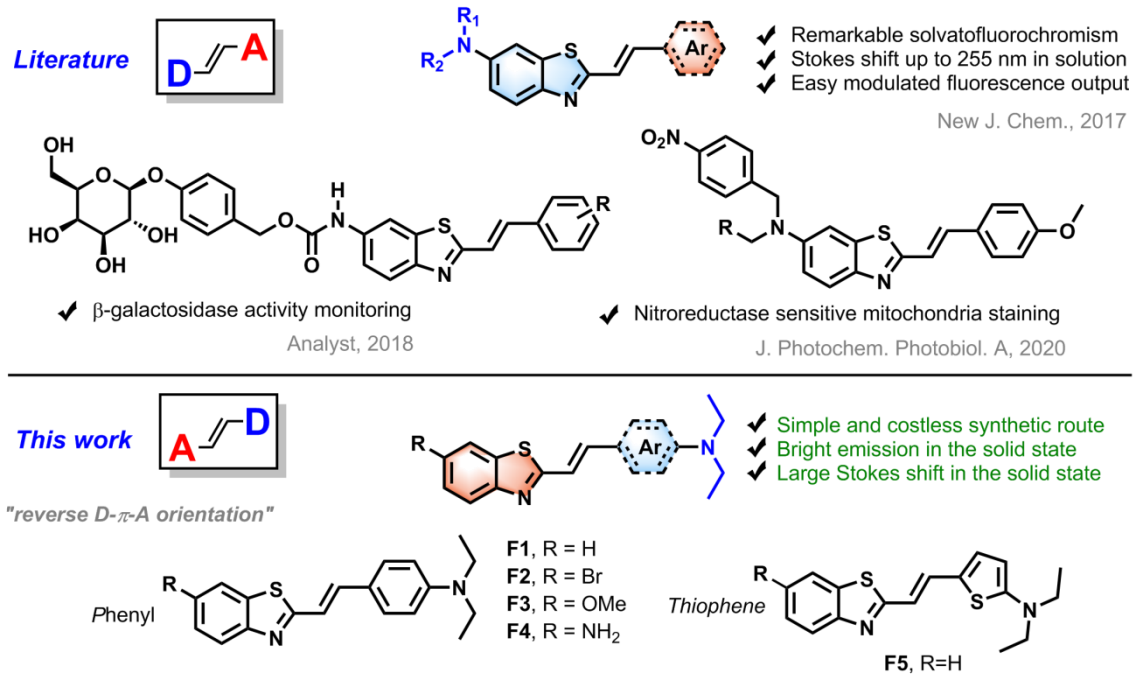

Figure 1. General benzothiazole-based styryl fluorophore reported by our group and the alternative framework described in the current work.

We report herein a simple and low-cost synthetic route to access the fluorogenic dyes **F1**-**F5** and the evaluation of their photophysical properties. The assessment of these fluorophores has enabled us to ascertain the effect of two types of modifications at the benzothiazole-based styryl backbone on the photophysics of these compounds:(i) decoration of the benzothiazole ring with different substituents modulating its electronic density (Figure 1, **F1**-**F4**), and (ii) the replacement of the phenyl scaffold by the electron-richer thienyl framework (Figure 1, **F1** *vs***F5**). Therefore, the photophysical characterization of these

fluorophores in solution and the solid state, was deeply studied using the support of TD-DFT calculations. We anticipate that conversely from the former fluorophore's series, these dyes disclose a single, remarkable, and bright fluorescence emission band in their solid-state, in addition to the expected moderate solvatochromic effect observed in both absorption and the emission bands. Indeed, solid-state emissive fluorophores have found potential applications in several advanced technological fields such as sensing [17], organic light emitting diodes (OLEDs) [18,19], security printing technologies [20], data recording and storage [21], and solid-state laser dyes [22]. Thus, we believe that the study described herein may unlock a branch of opportunities and foster a new basis for designing fluorescent tools exploiting this D-π-A styryl-benzothiazole framework; notably, robust, easy-tunable and chemically stable solid-state emissive fluorophores can be readily provided using a simple and scalable synthetic strategy.

2. Experimental

2.1 Materials and methods

All solvents for absorption and fluorescence experiments were of spectroscopic grade. All chemical reagents were obtained from commercial suppliers (Aldrich, Across, Alfa Aesar) and were used without further purification. The reactions were monitored by thin-layer chromatography (TLC, Merck silica gel 60 F254 plates) and visualized by UV irradiation (254 & 365 nm) and/or by spraying with an appropriate staining agent. Column chromatography was performed with flash silica gel (40–63 mm). ^{1}H (400 MHz) and ^{13}C{1H} (101 MHz) NMR spectra were recorded on 400 MHz Bruker Advance with samples dissolved in CD_2Cl_2-d_2, with the solvent residual signals as internal references: 5.32 ppm (^{1}H NMR) and 53.84 ppm (^{13}C NMR). Chemical shifts (δ) are given in ppm to the nearest 0.01 (^{1}H) or 0.1 ppm (^{13}C). The coupling constants (*J*) are given in Hertz (Hz). The signals are reported as follows: chemical shift, multiplicity (s = singlet, d = doublet, t = triplet, m = multiplet, dd = doublet of doublets, br s = broad singlet), coupling constants (*J*) and integration. High-Resolution Mass Spectra (HRMS) were recorded on a Micromass Q-Tof spectrometer, using electrospray ionization (ESI) at a resolution of 140 000 at m/z 200. UV-vis absorption spectra were obtained

using a Shimadzu UV-2450 spectrophotometer. Steady-state fluorescence spectra were obtained using a Shimadzu RF-5301PC spectrofluorometer. For emission spectra, the absorption maximum wavelength as excitation radiation was used. The quantum yield of fluorescence was measured at 25 °C using Coumarin 153 in ethanol as the quantum yield standard [23]. Diffuse reflectance ultraviolet-visible (DRUV) spectra were recorded by a UV-Vis spectrophotometer (Shimadzu UV-2450) equipped with an ISR-2200 integrating sphere attachment in a spectral range of 250−850 nm using $BaSO_4$ (Wako Pure Chemical Industries, Ltd) as a reference. Steady-state fluorescence spectra in the solid-state were measured on a Shimadzu spectrofluorometer model RF-5301PC equipped with a Xenon lamp. A solid sample holder was used, where the light beam was irradiated to the sample at an angle of ca. 45° to limit the reflected excitation beam from the emission monochromator. In these experiments, the samples were treated as powder. All measurements were carried out at 25 °C.

2.2 General synthesis of the fluorophores (**F1**-**F5**)

Precursors 2-methylbenzothiazoles **1**-**4** (1.0 equiv.), potassium tert-butoxide (1.0 equiv.), and the aldehyde **5** (or **6** when using benzothiazole **1**) (1.0 equiv.) were stirred in DMSO (0.2 M), for 2 hours at room temperature. The reaction mixture was diluted with ethyl acetate and washed with water (3 × 100 mL). The organic layer was dried over magnesium sulfate, filtered and the volatiles were removed under reduced pressure. The crude was purified by flash column chromatography on silica gel using cyclohexane/ethyl acetate mixtures as the eluents. Finally, recrystallization from methanol afforded the desired fluorophores as bright solids.

(*E*)-4-(2-(Benzo[*d*]thiazol-2-yl)vinyl)-*N*,*N*-diethylaniline (**F1**). The compound was prepared using benzothiazole **1** (75 mg, 0.5 mmol), potassium tert-butoxide (56 mg, 0.5 mmol), and aldehyde **5** (88 mg, 0.5 mmol). Flash chromatography was performed using 80/20 cyclohexane/ethyl acetate mixtures. Yield: 72% (111.1 mg). ^{1}H NMR (400 MHz, CD_2Cl_2-d_2) δ 7.89 (d, *J*=8.1 Hz, 1H), 7.84 (d, *J*=7.9 Hz, 1H), 7.47-7.41 (m, 4H), 7.32 (t, *J*=7.6 Hz, 1H), 7.15 (d, *J*=16.0 Hz, 1H), 6.68 (d, *J*=8.5 Hz, 2H), 3.41 (q, *J*=7.0 Hz, 4H), 1.19 (t, *J*=7.0 Hz, 6H). ^{13}C NMR (101

MHz, CD_2Cl_2-d_2) δ 168.6, 154.6, 149.3, 138.7, 134.6, 129.55, 126.4, 124.9, 122.6, 122.6, 121.8, 116.8, 111.8, 44.8, 12.8. HRMS (ESI) m/z: $[M+H]^+$ calc. for $C_{19}H_{21}N_2S$ 309.1425; found 309.1401.

(*E*)-4-(2-(6-Bromobenzo[*d*]thiazol-2-yl)vinyl)-*N*,*N*-diethylaniline (**F2**). The compound was prepared using benzothiazole **2** (114 mg, 0.5 mmol), potassium tert-butoxide (56 mg, 0.5 mmol), and aldehyde **5** (88 mg, 0.5 mmol). Flash chromatography was performed using 80/20 cyclohexane/ethyl acetate mixtures. Yield: 57% (109.9 mg). ^{1}H NMR (400 MHz, CD_2Cl_2-d_2) δ 7.96 (d, *J*=1.9 Hz, 1H), 7.74 (d, *J*=8.6 Hz, 1H), 7.52 (dd, *J*=8.6 Hz and 2.0 Hz, 1H), 7.46-7.42 (m, 2H), 7.12 (d, *J*=16.0 Hz, 1H), 6.68 (d, *J*=8.9 Hz, 2H), 3.41 (q, *J*=7.1 Hz, 4H), 1.19 (t, *J*=7.1 Hz, 6H). ^{13}C NMR (101 MHz, CD_2Cl_2-d_2) δ 169.2, 153.6, 149.4, 139.4, 136.4, 129.7, 129.7, 124.3, 123.7, 122.4, 118.1, 116.3, 111.8, 44.9, 12.8. HRMS (ESI) m/z: $[M+H]^+$ calc. for $C_{19}H_{20}BrN_2S$ 387.0531; found 387.0503.

(*E*)-*N*,*N*-Diethyl-4-(2-(6-methoxybenzo[*d*]thiazol-2-yl)vinyl)aniline (**F3**). The compound was prepared using benzothiazole **3** (90 mg, 0.5 mmol), potassium tert-butoxide (56 mg, 0.5 mmol), and aldehyde **5** (88 mg, 0.5 mmol). Flash chromatography was performed using 80/20 cyclohexane/ethyl acetate mixtures. Yield: 89% (150.7 mg). ^{1}H NMR (400 MHz, CD_2Cl_2-d_2) δ 7.77 (d, *J*=8.9 Hz, 1H), 7.43 (d, *J*=8.8 Hz, 2H), 7.35-7.31 (m, 2H), 7.11 (d, *J*=16.1 Hz, 1H), 7.02 (dd, *J*=8.9 Hz and 2.6 Hz, 1H), 6.68 (d, *J* = 8.9 Hz, 2H), 3.86 (s, 3H), 3.40 (q, *J* = 7.1 Hz, 4H), 1.19 (t, *J* = 7.1 Hz, 6H). ^{13}C NMR (101 MHz, CD_2Cl_2-d_2) δ 166.2, 157.9, 149.1, 137.7, 135.9, 129.4, 129.33, 123.1, 122.8, 117.1, 115.3, 111.8, 104.6, 56.2, 44.8, 12.8. HRMS (ESI) m/z: $[M+H]^+$ calc. for $C_{20}H_{23}N_2OS$ 339.1531; found 339.1506.

(*E*)-2-(4-(Diethylamino)styryl)benzo[*d*]thiazol-6-amine (**F4**). The compound was prepared using benzothiazole **4** (82 mg, 0.5 mmol), potassium tert-butoxide (56 mg, 0.5 mmol), and aldehyde **5** (88 mg, 0.5 mmol). Flash chromatography was performed using 80/20 cyclohexane/ethyl acetate mixtures. Yield: 54% (87.6 mg). ^{1}H NMR (400 MHz, CD_2Cl_2-d_2) δ 7.64 (d, *J*=8.6 Hz, 1H), 7.42 (d, *J*=8.9 Hz, 2H), 7.27 (d, *J*=16.1 Hz, 1H), 7.11-7.07 (m, 2H), 6.78 (dd, *J*=8.6 Hz and 2.3 Hz,

1H), 6.67 (d, *J*=8.9 Hz, 2H), 3.88 (br s, 2H), 3.40 (q, *J*=7.1 Hz, 4H), 1.18 (t, *J*=7.1 Hz, 6H). ^{13}C NMR (101 MHz, CD_2Cl_2-d_2) δ 186.3, 183.6, 164.3, 148.9, 147.8, 145.1, 136.9, 136.3, 129.2, 123.2, 122.9, 117.3, 115.4, 111.8, 105.9, 44.8, 12.8. HRMS (ESI) m/z: $[M+H]^+$ calc. for $C_{19}H_{22}N_3S$ 324.1534; found 324.1511.

(*E*)-5-(2-(Benzo[*d*]thiazol-2-yl)vinyl)-*N*,*N*-diethylthiophen-2-amine (**F5**). The compound was prepared using benzothiazole **1** (44.7 mg, 0.3 mmol), potassium tert-butoxide (33.6 mg, 0.3 mmol), and aldehyde **6** (55.0 mg, 0.3 mmol). Flash chromatography was performed using 80/20 cyclohexane/ethyl acetate mixtures. Yield: 41% (38.4 mg). ^{1}H NMR (400 MHz, DMSO-d_6) δ 7.97 (d, *J*=7.8 Hz, 1H), 7.82 (d, *J*=8.0 Hz, 1H), 7.63 (d, *J*=15.5 Hz, 1H), 7.47-7.40 (m, 1H), 7.36-7.27 (m, 1H), 7.18 (d, *J*=4.1 Hz, 1H), 6.58 (d, *J*=15.5 Hz, 1H), 5.92 (d, *J*=4.1 Hz, 1H), 3.37 (q, *J*=7.1 Hz, 4H), 1.17 (t, *J*=7.1 Hz, 6H). ^{13}C NMR (125 MHz, DMSO-d_6) 166.9, 159.3, 153.8, 134.4, 133.5, 131.9, 126.2, 124.3, 121.9, 121.8, 121.5, 111.9, 101.7, 46.6, 12.1. HRMS (ESI) m/z: $[M+H]^+$ calc. for $C_{17}H_{19}N_2S_2$ 315.0990; found 315.0966.

2.2 Theoretical Calculations

The structures were determined theoretically after geometry optimization at the density functional theory (DFT) level using the functional PBE0 [24], and the basis set aug-cc-pVDZ [25-30]. The vibrational frequencies were calculated using the same configuration to investigate the minimum global structure. To investigate solvatochromism, the ground state geometry was optimized with the conductor-like polarizable continuum model (CPCM) [31]. The vertical excitation was obtained using the same level of calculation using the time-dependent DFT method (TD-DFT). All calculations used the software ORCA version 5.0.3 [32,33], Gabedit 2.5.1 software [34], and Avogadro 1.2 software [35].

3. Results and discussion

3.1 Synthesis

The preparation of fluorophores **F1**-**F5** was accomplished by assembling the benzothiazole or substituted benzothiazole scaffolds and 4-*N*,*N'*-diethylaminostyryl, or 5-*N*,*N'*-diethylaminovinyl thienyl frameworks (Scheme 1).

Here, the synthetic route to form the target styryl framework was carried out *via* Knoevenagel condensation, using 2-methylbenzothiazole precursors **1**-**4** and the corresponding aromatic aldehydes, *N*,*N'*-diethylaminobenzaldehyde or 5-*N*,*N'*-diethylamino thienyl carboxaldehyde. The precursors were obtained from commercial sources or synthesized according to previously reported procedures [8,**Error! Bookmark not defined.**]. Firstly, we undertook the preparation of **F1**-**F4**. These dyes were prepared in DMSO, at room temperature, and in the presence of *t*BuOK as the base, using an equimolar amount of *N*,*N'*-diethylaminobenzaldehyde (**5**), and the corresponding 2-methylbenzothiazole precursor (**1**-**4**). Next, we finish this series by accessing fluorophore **F5** using 5-*N*,*N'*-diethylaminothienyl carboxaldehyde (**6**) [36], and 2-methylbenzothiazole (**1**) precursors, applying the custom reaction condition. The obtained fluorophores **F1**-**F5** were isolated in satisfactory yields (41-89%) after purification by flash chromatography and finally crystallized from pure methanol to ensure high purity.

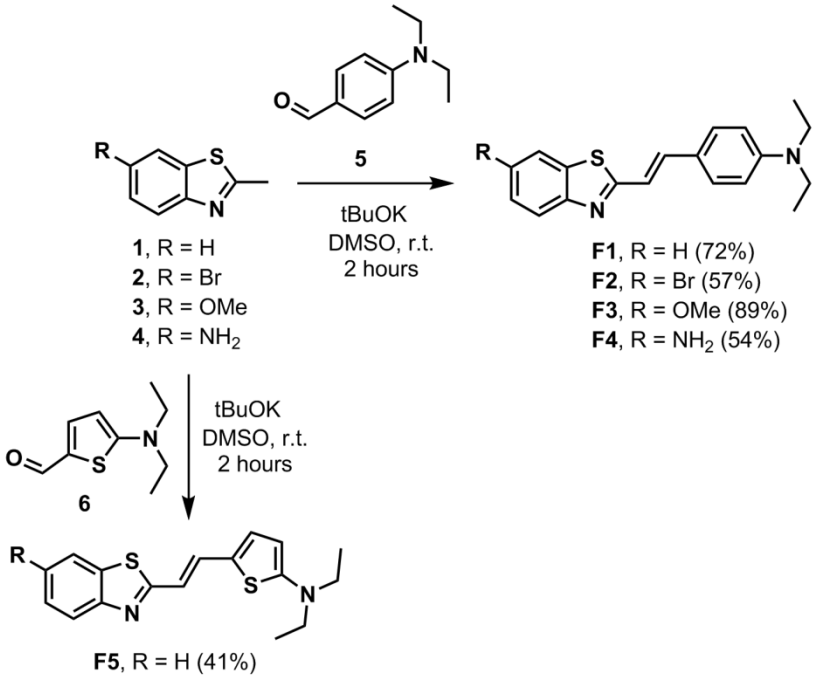

Scheme 1. Synthetic route to access the target benzothiazole-based styryl fluorophores **F1**-**F5**.

3.2 Photophysical characterization

The UV-Vis absorption and fluorescence emission spectra of the benzothiazole-based styryl fluorophores **F1**-**F5** are presented in Figures 2 and

3, where the compounds were investigated in solutions of different organic solvents. The relevant photophysical data are summarized in Table 1.

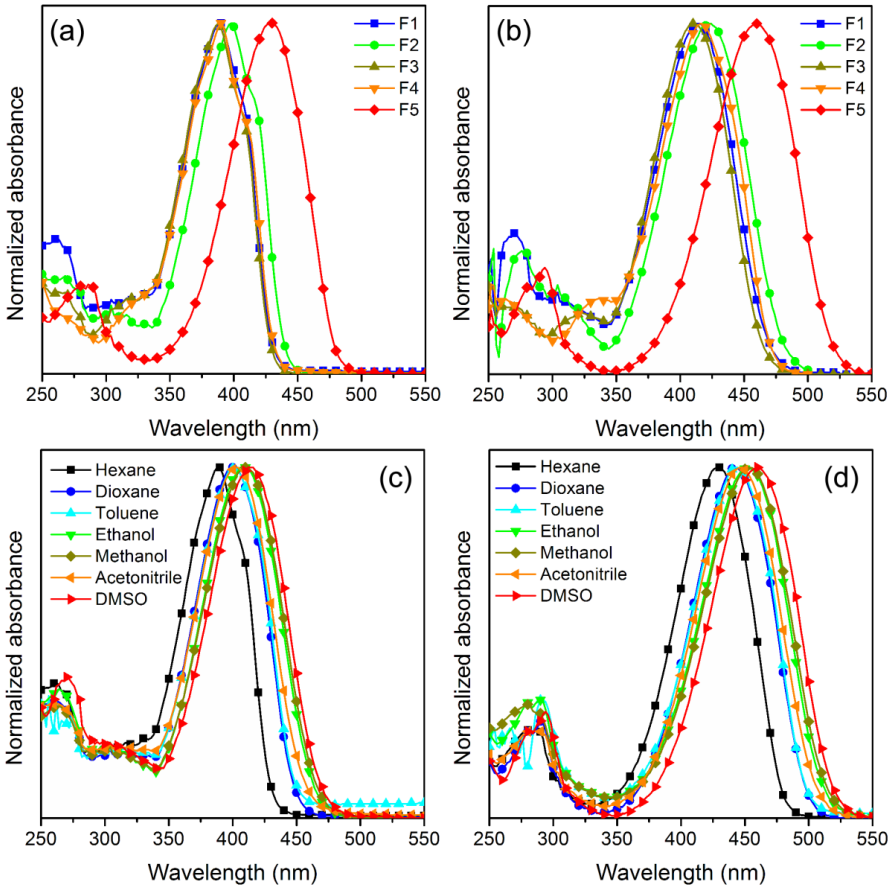

Figure 2. Normalized UV-Vis absorption spectra in solution (ca. 10^{-5} M) of fluorophores **F1**-**F5** in (a) hexane and (b) DMSO, and (c) **F1** and (d) **F5** in different organic solvents.

Figure 2a depicts the UV-Vis spectra of all compounds in hexane, where it was observed that compounds **F1**, **F3**, and **F4** presented the absorption maxima located in the same region (388-390 nm). On the other hand, compound **F2** showed a redshifted absorption maximum (398 nm) compared to previous compounds. This observation is due to the electronegativity of the halogen-atom, as already reported in the literature [37,38]. Indeed, theoretical calculations (see Section 3.3) indicated a charge transfer character from the amino moiety towards the aromatic frames, an effect magnified by the bromine substituent in **F2** in comparison to **F3**.

In addition, thienyl-based fluorophore **F5** presented an absorption maximum at 429 nm, indicating that the aromatic framework (phenyl and thienyl) plays a significant role in their photophysics. Compounds **F1**-**F5** showed similar behavior in DMSO (Figure 2b), but presented absorption maxima values redshifted (410-460 nm) in comparison to hexane, due to the greater polar character of this solvent. Taking compounds **F1** and **F5** as models, a positive solvatochromic effect could be observed ($\Delta\lambda_{abs}$: 26 nm to **F1**and 32 nm to **F5**) (Figures 2c-d), emphasized by a gradual redshift of the absorption maxima as the solvent polarity increases. This latter indicates for these compounds that the dipole moment in the ground state seems to be smaller than in the excited state. It is worthy to note that the same trend was observed for compounds **F2-F4**(Figures S16-S18). In this investigation, it is also believed that in ethanol and methanol, the specific interactions between fluorophore and solvent promoted by hydrogen bonding in this media also play a role in the observed red-shifted absorption bands [39].

Table 1. Photophysical data of **F1**-**F5** where λ_{abs} is the absorption maxima (nm), ε is the molar extinction coefficient (10^4 $M^{-1}\cdot cm^{-1}$), λ_{em} is the emission maxima, *f* is the calculated oscillator strength, k_e^0 is the calculated radiative rate constant (10^8 s^{-1}), τ^0 is the calculated pure radiative lifetime (ns), λ_{em} is the emission maxima (nm), $\Delta\lambda_{ST}$ is the Stokes shift (nm/cm^{-1}), and QY is the fluorescence quantum yield.

Compound	Solvent	λ_{abs}	ε	λ_{em}	$\Delta\lambda_{ST}$	*f*	k_e^0	τ^0	QY
	Hexane	388	2.89	456	68/3843	0.53	3.53	2.83	0.25
	1,4-Dioxane	400	2.80	475	75/3947	0.53	3.34	3.00	0.32
	Toluene	402	3.01	474	72/3779	0.55	3.38	2.96	0.30
F1	Ethanol	408	2.43	504	96/4669	0.48	2.86	3.50	0.42
	Methanol	410	3.64	515	105/4973	0.72	4.31	2.32	0.24
	Acetonitrile	402	3.09	509	107/5229	0.62	3.79	2.64	0.29
	DMSO	414	1.73	517	103/4812	0.34	1.97	5.09	0.60
	Hexane	398	2.06	461	63/3434	0.36	2.26	4.42	0.22
	1,4-Dioxane	408	1.55	488	80/4018	0.27	1.58	6.34	0.45
	Toluene	408	1.79	472	64/3323	0.34	2.01	4.97	0.24
F2	Ethanol	416	2.18	515	99/4621	0.44	2.56	3.91	0.28
	Methanol	416	2.03	525	109/4991	0.42	2.39	4.18	0.23
	Acetonitrile	410	1.98	519	109/5122	0.40	2.38	4.21	0.32
	DMSO	422	1.76	529	107/4793	0.33	1.86	5.38	0.58
	Hexane	388	3.97	450	62/3551	0.77	5.09	1.97	0.48
	1,4-Dioxane	398	3.41	471	73/3894	0.69	4.33	2.31	0.43
	Toluene	400	3.25	471	71/3769	0.65	4.07	2.45	0.41
F3	Ethanol	406	3.29	499	93/4590	0.70	4.25	2.35	0.31
	Methanol	408	2.91	510	102/4902	0.62	3.73	2.68	0.23
	Acetonitrile	400	3.83	500	100/5000	0.80	4.97	2.01	0.29
	DMSO	410	4.02	512	102/4859	0.82	4.86	2.06	0.54
	Hexane	390	3.48	455	65/3663	0.67	4.43	2.26	0.81
	1,4-Dioxane	402	2.81	474	72/3779	0.57	3.55	2.82	0.74
	Toluene	402	4.30	471	69/3644	0.88	5.43	1.84	0.48
F4	Ethanol	410	2.20	500	90/4390	0.48	2.84	3.52	0.34
	Methanol	410	3.99	504	94/4549	0.88	5.25	1.90	0.19
	Acetonitrile	404	3.15	494	90/4510	0.64	3.94	2.54	0.33
	DMSO	416	3.80	502	86/4118	0.80	4.59	2.18	0.55
	Hexane	429	2.29	498	69/3230	0.39	2.13	4.69	0.06
	1,4-Dioxane	444	2.63	520	76/3292	0.45	2.29	4.37	0.11
	Toluene	444	3.37	513	69/3029	0.59	2.98	3.35	0.09
F5	Ethanol	452	2.89	533	81/3362	0.56	2.74	3.64	0.04
	Methanol	454	4.10	539	85/3474	0.75	3.66	2.73	0.04
	Acetonitrile	448	2.49	537	89/3699	0.44	2.23	4.49	0.06
	DMSO	461	2.86	545	84/3343	0.49	2.32	4.32	0.09

The molar absorptivity coefficient (~10^4 $M^{-1}\cdot cm^{-1}$), as well as the calculated radiative rate constant (~10^8 s^{-1}) values obtained from the Beer-Lambert law and the Strickler-Berg relations, respectively, indicated that the absorption maxima are spin- and symmetry-allowed electronic transitions, which could be related to $^1\pi\pi^*$ transitions. The mentioned Strickler-Berg relations are described in Equations (1) and (2) and were also used to calculate the oscillator strength (f_e) and the theoretical rate constant for emission (k_e^0). In these equations, ε is the experimental extinction coefficient and the integral is the area under the absorption curve from a plot of ε ($M^{-1}\cdot cm^{-1}$) vs the wavelength in wavenumber (cm^{-1}), corresponding to a single electron oscillator [40]. In addition, k_e^0 was used to calculate the pure radiative lifetime τ^0, defined as $1/k_e^0$ [41] (Table 1).

$$f_e \approx 4.3x10^{-9} \int \varepsilon d\bar{\nu} \qquad (1)$$

$$k_e^0 \approx 2.88x10^{-9} \bar{\nu}_0^2 \int \varepsilon d\bar{\nu} \qquad (2)$$

Values to the oscillator strength of around 0.6 were obtained, an indication of highly probable electronic transitions. Pure radiative lifetime values between the compounds in all studied solvents showed the same order of magnitude (~10^{-9} s), indicating that even presenting different substituents and conjugated frameworks, the absorptions of the studied compounds populated a similar excited state.

The emission curves were obtained by exciting the compounds at the absorption maxima wavelengths. The relevant data from fluorescence emissions are also summarized in Table 1. Figure 3a depicts the steady-state fluorescence emission spectra of all compounds in hexane, where all fluorophores presented structured spectra. The fluorophores containing the phenyl moiety showed emission maxima in a very close range (450-461 nm). On the other hand, as already observed in the UV-Vis spectra, compound **F5** showed a redshifted emission (498 nm) compared with its parent compounds. In more polar solvents (Figure 3b, DMSO), the change in the electronic character of the substituent affects the photophysical behavior of the fluorophores, where the compounds **F1**-**F4** showed emission maxima in a wider

window (502-529 nm). Once again, compound **F5** presented its emission shifted to a longer wavelength (545 nm). A more pronounced positive solvatochromic effect is observed in the emission spectra (Figures 3c-d) (**F1**: 62 nm and **F5**: 47 nm), which may indicate that these compounds have larger dipole moments in the excited state. A relatively large Stokes shift could be calculated for all compounds (3029-5168 cm^{-1}), which could probably be related to an intramolecular charge transfer mechanism in these compounds. The additional compounds showed similar photophysical results (Figures S19-S21). The phenyl-based fluorophores (**F1**-**F4**) presented relatively high fluorescence quantum yields (0.22-0.81) whereas compound **F5** showed, on average, 10 times lower values. This indicates that the presence of the thienyl group in the fluorophore favors a very efficient non-radiative excited-state deactivation channel. It was also observed that the emission spectra were a mirror image of the excitation spectra (Figure S22) and that the excitation spectra presented a quite similar shape and position compared to the respective UV-Vis spectra.

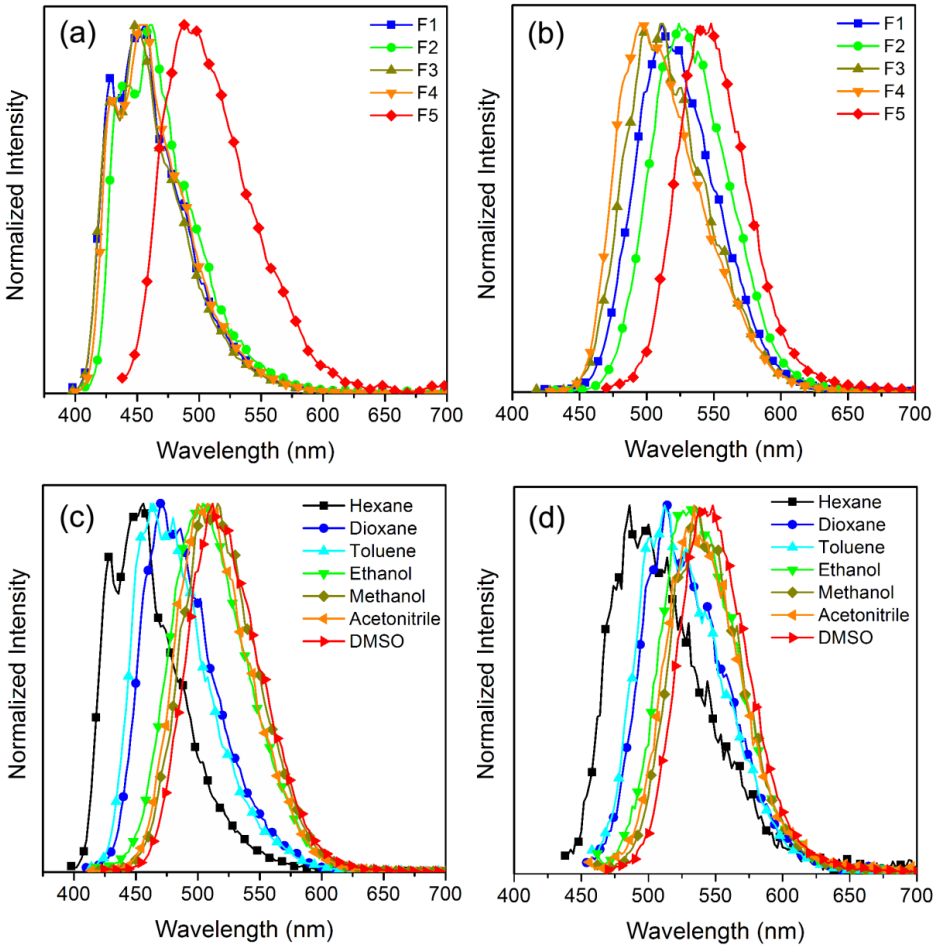

Figure 3. Normalized steady-state fluorescence emission spectra in solution (ca. 10^{-5} M) of fluorophores **F1**-**F5** in (a) hexane and (b) DMSO, and (c) **F1** and (d) **F5** in different organic solvents.

To estimate the charge distribution in the ground and excited states, the difference in the dipole moment between the excited and ground states ($\Delta\mu$) was achieved by the Lippert-Mataga model, which is an approximate form to compare solvents properties and the energy difference between absorption and emission maxima [42-45]. This correlation compares the solvatochromic shifts from the Stokes shift versus the orientation polarization function (Δf), which is obtained according to Equation (3):

$$\Delta f = \frac{\varepsilon-1}{2\varepsilon+1} - \frac{n^2-1}{2n^2+1}, \quad (3)$$

where ε is the dielectric constant and *n* the refraction index (Table S1). In this plot, a linear relation of the Stokes shift versus the solvent polarity function indicates the internal charge transfer character. The slopes *m* obtained from linear plots, and the variation of dipole moment $\Delta\mu$, is expressed as Equation (4):

$$\Delta\mu = \sqrt{\frac{mhca^3}{2}}, \quad (4)$$

where *h* is the Planck constant, *c*is the velocity light and *a* is the Onsager cavity radius attribute to the compound, which can be calculated from Equation (5), where M is the molar mass, ρ is the density predicted using ACD/ChemSketch software and N is the Avogadro's number [43].

$$a = \left(\frac{3M}{4\pi\rho N}\right)^{1/3}, \quad (5)$$

The results of the Lippert-Mataga model are presented in Figure 4 and the relevant data are summarized in Table 2. The obtained curves disclosed a positive slope, which effectively confirms that the dipole moment of these compounds increases in the excited state. Thus, this result corroborates with the more pronounced positive solvatochromic effect in the emission spectra when compared to the absorption spectra.

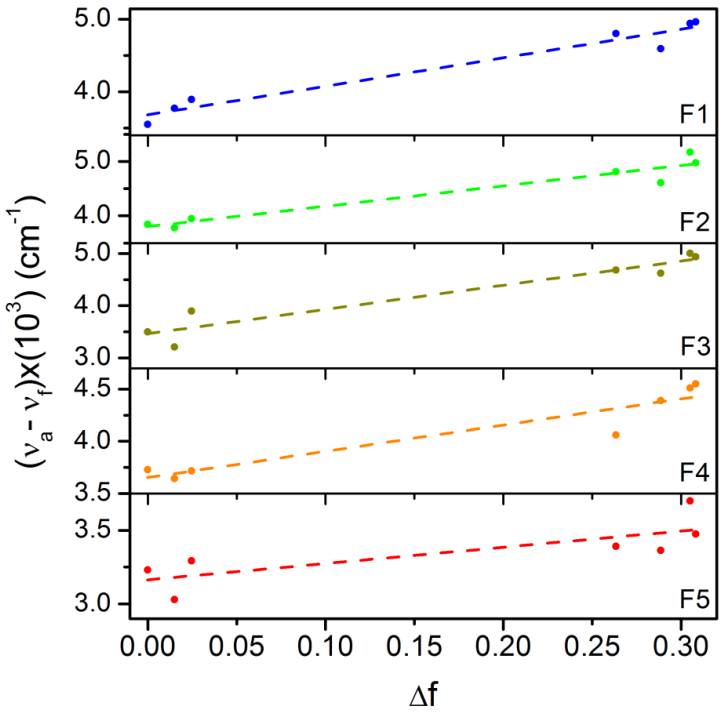

Figure 4. The Lippert-Mataga plotting $\bar{\nu}_a - \bar{\nu}_f \, vs. \Delta f$ and linear fitting.

Table 2. The Slope and coefficient of correlation, M is the molar mass (g·mol^{-1}), ρ is the predicted density (g·cm^{-3}), a is the Onsager cavity radius in angstrom, and Δμis the variation of dipole moment between ground and excited state.

Compound	Slope	Pearson	M	ρ	a	Δμ
F1	3925	0.98	308.44	1.184	4.69	6.34
F2	3742	0.97	387.34	1.400	4.79	6.38
F3	4633	0.96	338.47	1.189	4.83	7.21
F4	2517	0.95	323.45	1.231	4.71	5.10
F5	1071	0.79	314.47	1.258	4.63	3.25

The photophysics of the benzothiazole-based styryl fluorophores **F1**-**F5** was also investigated in the solid-state (Figure 5). As shown in Figure 5a, the compounds presented broad absorption bands, with maxima located at a region similar to those observed in the solution (~400 nm). In addition, the DRUV spectra present an increase in the absorption intensity at longer wavelengths (above 500 nm), probably related to π–π stacking, which becomes much more significant in the solid state. The fluorescence emission in the solid-state is present in Figure 5b. The spectra were acquired using the excitation maxima as excitation wavelength (~475 nm). The compounds presented emission maxima

around 520 nm, with a relatively large Stokes shift, similarly to than observed in the solution. Once again, compound **F5** presented a redshifted emission located at 610 nm, indicating that the thienyl framework also plays a role in the solid-state photophysics of this compound.

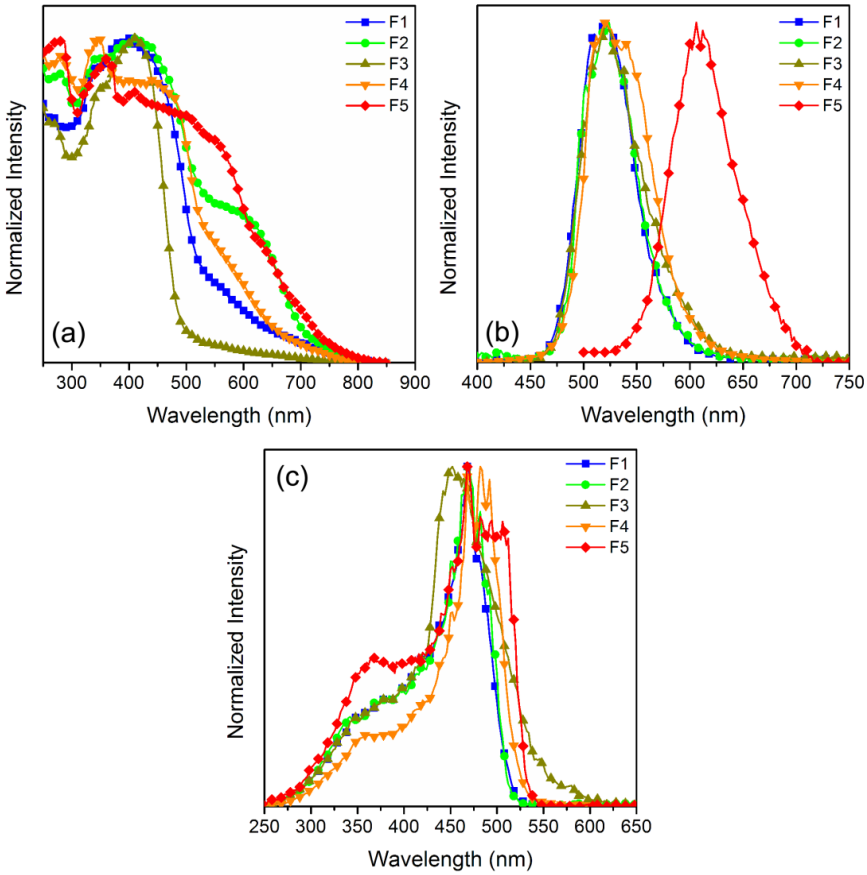

Figure 5. Normalized (a) DRUV, (b) fluorescence emission, and (c) excitation spectra of fluorophores **F1**-**F5** in the solid state.

3.3 DFT/TD-DFT calculation

The effect of bulk solvent polarity was approximated by the Conductor-like polarizable continuum model (CPCM) that correlates the properties of the solvents as the dielectric constant and refraction index to generate a potential surface and optimize the ground state geometries without considering specific interactions such as hydrogen bonds [46]. In the present study, the vertical excitation and frequencies of the molecules were treated with PBE0/aug-cc-pVDZ which was a functional and basis set that represented quite well the experimental data. In general, these styryl-based benzothiazoles show a planar

structure without major differences or torsions during the optimization with the simulated solvents (Figure 6). The calculated frequency predicts the infrared spectra of the studied compounds (Figure S23) and also indicates the quality of the optimization as there are no negative energies. The frequencies of the **F1-F5** show only positive values at the vacuum level and the most intense band in the infrared spectra refer to the phenyl **(F1-F4)** and thienyl **(F5)** groups, located between 1600-1500 cm^{-1} (Figure S24).

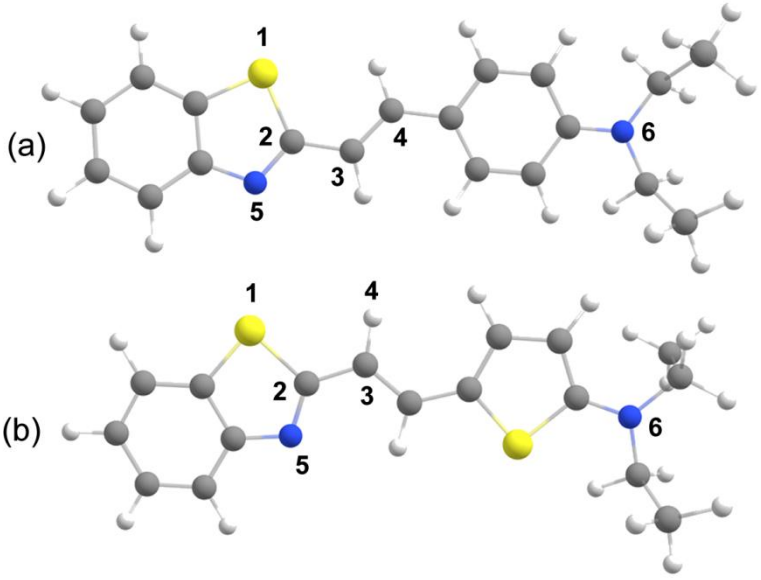

Figure 6. The optimized structures of (a) **F1** and (b) **F5** and their respective labeled atoms.

The UV-Vis theoretical absorption spectra of the **F1** and **F5**are presented in Figure 7. The compounds were investigated in different media using the CPCM model and compared to experimental spectra. The theoretical data are summarized in Table 3, where the differences between experimental and theoretical spectra are no more than 0.1 eV, and Tables S2-S6 show the comparison between the color of dyes obtained by complementary color to absorption spectra. In the UV-Vis spectra, all compounds have two absorption bands where the maximum intensity band is the HOMO-LUMO (Highest Occupied Molecular Orbital and Lowest Occupied Molecular Orbital) transition with a longer wavelength and the other band of minimum intensity with many high energy transitions. The difference between the maximum and minimum

bands is greater than ~100 nm (11000 cm^{-1}). These compounds showed a strong HOMO-LUMO transition, with over 96% attribution and with the next energy level ($HOMO_{-1}$-LUMO) being very high and with lower oscillator strength (Figure 8 and Figure S25).

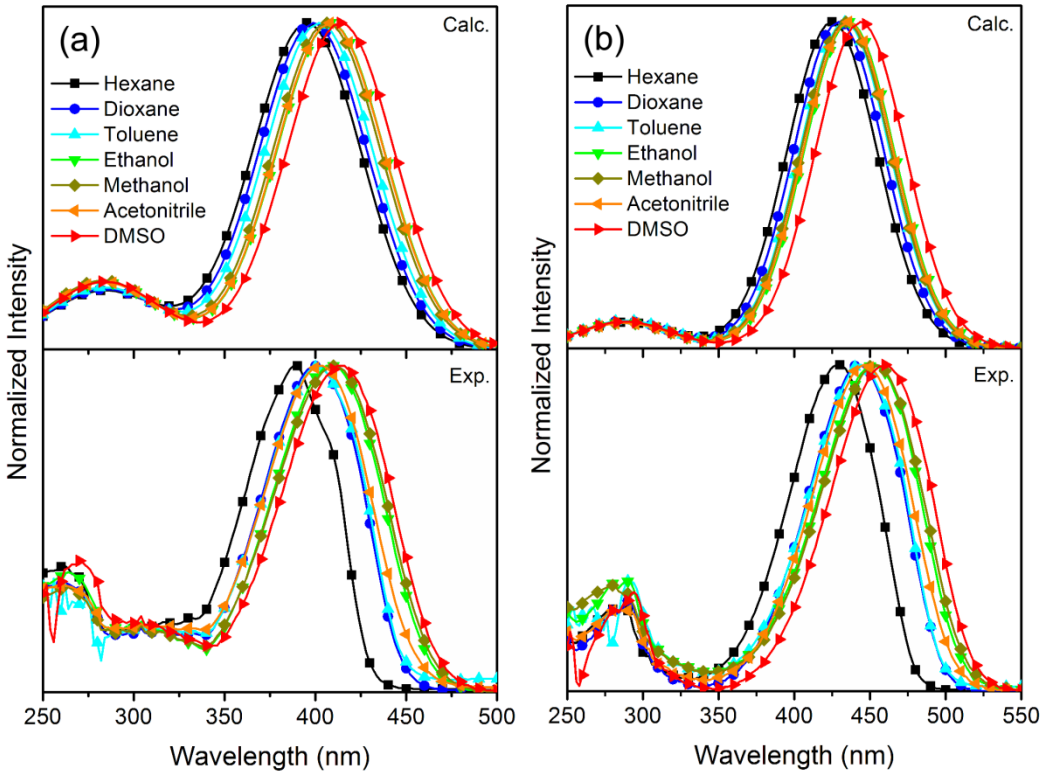

Figure 7. UV-Vis spectra experimental (Exp.) and theoretical (Calc.) with 35 nm of the half widths in the Gaussian adjust based on the experimental values of fluorophores **F1**-**F5** (a-b respectively).

Table 3. Theoretical data using PBE0/aug-cc-pVDZ, where λ_{calc} and λ_{exp} are the calculated and experimental absorption maxima (nm), ΔE is the energy difference between λ_{calc} and λ_{exp} (eV), and *f* is the oscillator strength and assignment of HOMO-LUMO transition.

Compound	Solvent	λ_{calc}	λ_{abs}	ΔE	*f*	Assignment H→L
	Hexane	395	388	0.06	0.94	97%
	1,4-Dioxane	399	400	0.01	0.97	97%
	Toluene	402	402	0.00	1.01	97%
F1	Ethanol	408	408	0.00	0.91	97%
	Methanol	407	410	0.02	0.88	97%
	Acetonitrile	408	402	0.05	0.89	97%
	DMSO	414	414	0.00	0.98	97%
	Hexane	403	398	0.04	1.09	97%
	1,4-Dioxane	407	408	0.01	1.12	97%
	Toluene	410	408	0.01	1.16	97%
F2	Ethanol	416	416	0.00	1.05	97%
	Methanol	415	416	0.01	1.03	97%
	Acetonitrile	416	410	0.04	1.04	97%
	DMSO	422	422	0.00	1.13	97%
	Hexane	396	388	0.06	1.04	97%
	1,4-Dioxane	399	398	0.01	1.07	97%
	Toluene	402	400	0.02	1.11	97%
F3	Ethanol	407	406	0.01	1.01	97%
	Methanol	406	408	0.01	0.99	97%
	Acetonitrile	407	400	0.05	1.00	97%
	DMSO	412	410	0.01	1.09	97%
	Hexane	401	390	0.09	1.03	97%
	1,4-Dioxane	404	402	0.02	1.06	97%
	Toluene	407	402	0.04	1.10	97%
F4	Ethanol	412	410	0.01	0.99	97%
	Methanol	411	410	0.01	0.97	97%
	Acetonitrile	411	404	0.05	0.98	97%
	DMSO	417	416	0.01	1.08	97%
	Hexane	425	429	0.03	0.82	97%
	1,4-Dioxane	429	444	0.10	0.85	97%
	Toluene	433	444	0.07	0.89	97%
F5	Ethanol	436	452	0.10	0.81	96%
	Methanol	434	454	0.13	0.78	96%
	Acetonitrile	436	448	0.08	0.80	96%
	DMSO	444	461	0.10	0.88	97%

The frontier molecular orbitals with HOMO-LUMO are represented in Figures 8 and Figure S26 with different solvents. From HOMO and LUMO orbitals, the electronic density is greater in the N6 group (-NEt_2) at the HOMO level, and decreases at the LUMO level, distributing the electronic density throughout the molecule. As observed, the energy level of the LUMOs

decreases from the vacuum to DMSO ($\Delta E_{vacuum\text{-}DMSO}$: **F1**: 0.212, **F2**: 0.130, **F3**: 0.244, **F4**: 0.265, and **F5**: 0.222), and the HOMOs ($\Delta E_{vacuum\text{-}DMSO}$: **F1**: 0.020, **F2**: 0.092, **F3**: 0.052, **F4**: 0.085, and **F5**: 0.016) almost do not present any energy variation. These results are in agreement with the Lippert-Mataga model which reveals that the dipole moment difference is positive due to the higher solvent-induced stabilization in the excited state. It is possible to observe on the frontier molecular orbitals a lowering of electronic density over the amino group from HOMOs to LUMOs orbitals, indicating a certain charge transfer character on the systems that further auxiliate on the explanation of the observed spectral features. Finally, the Molecular Electrostatic Potentials maps (MEP) show a high electronic density over the nitrogen from the benzothiazole moiety and the amino substituents (Figure S27), the possible regions for the occurrence of intermolecular hydrogen bonds with the protic solvents that contribute to the observed solvatochromic effects.

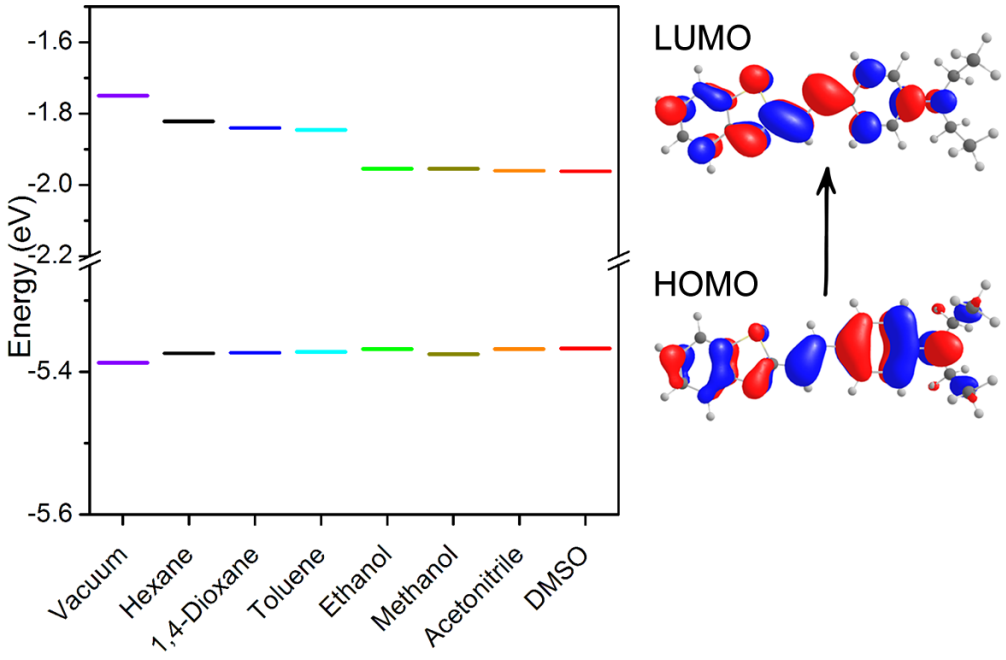

Figure 8. The energy level diagram of the **F1** compound in all solvents, and the electronic density of the HOMO-LUMO. The LUMO energy level decrease with an increased dielectric constant of the solvent.

4. Conclusions

The synthesis of new benzothiazole-based styryl fluorophores was performed using a straightforward and high-yielding route. These compounds presented a positive solvatochromic effect in both absorption and emission spectra, and high fluorescence quantum yield. The DFT/TD-DFT with the CPCM method enables to obtain results close to experimental data with an energy difference of less than 0.1 eV. The versatility of these compounds, featuring high fluorescence quantum yield in the solution and in solid state, high chemical stability, and pronounced solvafluorochromism in solution, can pave new routes for accessing specific probes and new analogs with optimal features for biological and optoelectronic applications.

Conflicts of interest

The authors have declared no conflicts of interest.

Acknowledgments

This work was supported by CNRS, University of Côte d'Azur, CAPES (fellowship to MSF, process number 99999.0011495/2015-01). The authors would like to acknowledge FAPERGS (17/2551-0000968-1), CNPq (409855/2018-9, 305041/2017-7 and 305954/2019-9) and Coordenação de Aperfeiçoamento de Pessoal de Nível Superior - Brasil (CAPES) - Finance Code 001 for the financial support.

References

[1] Z. Liu, G. Li, Y. Wang, J. Li, Y. Mi, D. Zou, T. Li, Y. Wu, Quinoline-based ratiometric fluorescent probe for detection of physiological pH changes in aqueous solution and living cells. Talanta, 192 (2019), pp. 6-13.

[2] B. Ditmangklo, J. Taechalertpaisarn, K. Siriwong, T. Vilaivan, Clickable Styryl dyes for fluorescence labeling of pyrrolidinyl PNA Probes for the detection of base mutations in DNA. Org. Biomol. Chem., 17 (2019), pp. 9712-9725.

[3] V. Botti, A. Cesaretti, Ž . Ban, I. Crnolatac, G. Consiglio, F. Elisei, I. Piantanida, Fine structural tuning of styryl-based dyes for fluorescence

and CD-based sensing of various Ds-DNA/RNA sequences. Org. Biomol. Chem., 17 (2019), pp. 8243-8258.

[4] Q. Li, J.S. Lee, C. Ha, B.P. Chan, G. Yang, B.G. Wen, Y.T. Chang, Solid-phase synthesis of styryl dyes and their application as amyloid sensors. Angew. Chem. Int. Ed., 43 (2004), pp. 6331-6335.

[5] M. Collot, E. Boutant, K.T. Fam, L. Danglot, A.S. Klymchenko, Molecular tuning of styryl dyes leads to versatile and efficient plasma membrane probes for cell and tissue imaging. Bioconjug. Chem., 31 (2020), pp. 875-883.

[6] M. Chandrasekharam, T. Suresh, S.P. Singh, B. Priyanka, K. Bhanuprakash, A. Islam, L. Han, M.L. Kantam, Functionalized styryl bipyridine as a superior chelate for a ruthenium sensitizer in dye sensitized solar cells. Dalton Trans., 41 (2012), pp. 8770-8772.

[7] J.A. Mikroyannidis, D.V. Tsagkournos, P. Balraju, G.D. Sharma, Low band gap dyes based on 2-styryl-5-phenylazo-pyrrole: synthesis and application for efficient dye-sensitized solar cells. J. Power Sources, 196 (2011), pp. 4152-4161.

[8] M. Safir Filho, S. Fiorucci, A.R. Martin, R. Benhida, Design, synthesis and photophysical studies of styryl-based push-pull fluorophores with remarkable solvatofluorochromism. New J. Chem., 41 (2017), pp. 13760-13772.

[9] C.L. Fleming, S. Li, M. Grøtli, J. Andréasson, Shining new light on the spiropyran photoswitch: A photocage decides between cis- trans or spiro-merocyanine isomerization. J. Am. Chem. Soc., 140 (2018), pp. 14069-14072.

[10] I.A. Karpenko, Y. Niko, V.P. Yakubovskyi, A.O. Gerasov, D. Bonnet, Y.P. Kovtun, A.S. Klymchenko, Push-pull dioxaborine as fluorescent molecular rotor: Far-red fluorogenic probe for ligand-receptor interactions. J. Mater. Chem. C, 4 (2016), pp. 3002-3009.

[11] K. Pal, F. Chandra, S. Mallick, A.L. Koner, Effect of solvents and cyclodextrin complexation on acid-base and photophysical properties of dapoxyl dye. J. Photochem. Photobiol. A Chem., 306 (2015), pp. 47-54.

[12] S.H. Kim, J.H. Ryu, H.J. Choi, H.S. Kim, Electrochromic properties of new fluorophores containing triphenylamine moiety. Dyes Pigm., 64 (2005), pp. 279-281.

[13] L. McDonald, D. Dahal, M. Konopka, Q. Liu, Y. Pang, An NIR emitting styryl dye with large stokes shift to enable co-staining study on zebrafish neuromast hair cells. Bioorg. Chem., 89 (2019), 103040.

[14] M. Safir Filho, P. Dao, A.R. Martin, R. Benhida, Visualization of intracellular lipid droplets using lipophilic benzothiazole-based push-pull fluorophores at ultralow concentration. Dyes Pigm., 167 (2019), pp. 68-76.

[15] M. Safir Filho, P. Dao, M. Gesson, A.R. Martin, R. Benhida, Development of highly sensitive fluorescent probes for the detection of β-galactosidase activity - Application to the real-time monitoring of senescence in live cells. Analyst, 143 (2018), pp. 2680-2688.

[16] M. Safir Filho, P. Dao, A.R. Martin, R. Benhida, Nitroreductase sensitive styryl-benzothiazole profluorescent probes for the visualization of mitochondria under normoxic conditions. J. Photochem. Photobiol. A Chem., 396 (2020), 112528.

[17] L. Zhang, Y. Chen, J. Jiang, Solid state fluorescent functionalized-triphenylamine Bodipy detector for HCl vapor with high stability and absolute fluorescent quantum yield. Dyes Pigm., 124 (2016), pp. 110-119.

[18] L. Yao, S. Zhang, R. Wang, W. Li, F. Shen, B. Yang, Y. Ma, Highly efficient near-infrared organic light-emitting diode based on a butterfly-shaped donor-acceptor chromophore with strong solid-state fluorescence and a large proportion of radiative excitons. Angew. Chem. Int. Ed., 53 (2014), pp. 2119-2123.

[19] J. Tagare, S. Vaidyanathan, Recent development of phenanthroimidazole-based fluorophores for blue organic light-emitting diodes (OLEDs): An overview. J. Mater. Chem. C, 6 (2018), pp. 10138-10173.

[20] X. Hou, C. Ke, C.J. Bruns, P.R. McGonigal, R.B. Pettman, J.F. Stoddart, Tunable solid-state fluorescent materials for supramolecular encryption. Nat. Commun., 6 (2015), 6884.

[21] D. Wu, W. Gong, H. Yao, L. Huang, Z. Lin, Q. Ling, Highly efficient solid-state emission of diphenylfumaronitriles with full-color AIE, and application

in explosive sensing, data storage and WLEDs. Dyes Pigm., 172 (2020), 107829.

[22] K. Parafiniuk, L. Sznitko, J. Mysliwiec, Distributed feedback and random lasing in DCNP aggregates dispersed in a polymeric layer. Opt. Lett., 40 (2015), pp. 1552-1555.

[23] C. Würth, M. Grabolle, J. Pauli, M. Spieles, U. Resch-Genger, Relative and absolute determination of fluorescence quantum yields of transparent samples. Nat. Protoc., 8 (2013), pp. 1535-1550.

[24] J.P. Perdew, K. Burke, M. Ernzerhof, Generalized gradient approximation made simple. Phys. Rev. Lett., 77 (1996), pp.3865-3868.

[25] F. Weigend, Accurate coulomb-fitting basis sets for H to Rn. Phys. Chem. Chem. Phys., 8 (2006), pp. 1057-1065.

[26] S. Lehtola, C. Steigemann, M.J.T. Oliveira, M.A.L. Marques, Recent developments in LIBXC - A comprehensive library of functionals for density functional theory. SoftwareX, 7 (2018), pp. 1-5.

[27] E.F. Valeev, Libint: A library for the evaluation of molecular integrals of many-body operators over Gaussian functions. 2022. Available: http://libint.valeyev.net/.

[28] R. Izsák, F. Neese, W. Klopper, Robust fitting techniques in the chain of spheres approximation to the Fock exchange: The role of the complementary space. J. Chem. Phys., 139 (2013), 094111.

[29] R.A. Kendall, T.H. Dunning, R.J. Harrison, Electron affinities of the first-row atoms revisited. Systematic basis sets and wave functions. J. Chem. Phys., 96 (1992), pp.6796-6806.

[30] R. Izsák, F. Neese, An overlap fitted chain of spheres exchange method. J. Chem. Phys., 135 (2011), 144105.

[31] M. Garcia-Ratés, F. Neese, Efficient implementation of the analytical second derivatives of Hartree-Fock and hybrid DFT energies within the framework of the conductor-like polarizable continuum model. J. Comput. Chem., 40 (2019), pp. 1816-1828.

[32] F. Neese, F. Wennmohs, U. Becker, C. Riplinger, The ORCA quantum chemistry program package. J. Chem. Phys., 152 (2020), 224108.

[33] F. Neese, The ORCA program system. Wiley Interdiscip. Rev. Comput. Mol. Sci., 2 (2012), pp. 73-78.

[34] A. Allouche, Software news and updates gabedit - A graphical user interface for computational chemistry softwares. J. Comput. Chem., 32 (2012), pp. 174-182.

[35] R. López, Avogadro: An advanced semantic chemical editor, visualization, and analysis platform. Adv. Math., 262 (2014), pp. 476-483.

[36] P. Yan, A. Xie, M. Wei, L.M. Loew, Amino(oligo)thiophene-based environmentally sensitive biomembrane chromophores. J. Org. Chem., 73 (2008), pp. 6587-6594.

[37] X.F. Zhang, I. Zhang, L. Liu, Photophysics of halogenated fluoresceins: Involvement of both intramolecular electron transfer and heavy atom effect in the deactivation of excited states. Photochem. Photobiol., 86 (2010), pp. 492-498.

[38] E.S. Moraes, L.G.T.A. Duarte, J.C. Germino, T.D.Z. Atvars, Near attack conformation as strategy for ESIPT modulation for white-light generation. J. Phys. Chem. C, 124 (2020), pp. 22406-22415.

[39] S. Nigam, S. Rutan, Principles and applications of solvatochromism. Appl. Spectrosc., 55 (2001), pp. 362A-370A.

[40] S.J. Strickler, R.A. Berg, Relationship between absorption intensity and fluorescence lifetime of molecules. J. Chem. Phys., 37 (1962), pp. 814-822.

[41] N.J. Turro, J.C. Scaiano, V. Ramamurthy, In Principles of molecular photochemistry: An introduction, University Science Book, 1st ed., 2008.

[42] E. Lippert, W. Lüder, F. Moll, W. Nägele, H. Boos, H. Prigge, I. Seinbold-Blankenstein, Umwandlung von Elektronenanregungsenergie. Angew. Chem., 73 (1961), pp. 695-706.

[43] N. Pandey, N. Tewari, S. Pant, M.S. Mehata, Solvatochromism and estimation of ground and excited state dipole moments of 6-aminoquinoline. Spectrochim. Acta A, 267 (2022), 120498.

[44] L.G.T.A. Duarte, F.S. Rodembusch, T.D.Z. Atvars, R.G. Weiss, Experimental and theoretical investigation of excited-state intramolecular proton transfer processes of benzothiazole derivatives in amino-

polydimethylsiloxanes before and after cross-linking by CO_2. J. Phys. Chem. A, 124 (2020), pp. 288-299.

[45] J.R. Lakowicz (Author), Solvent and Environmental Effects. In Principles of Fluorescence Spectroscopy, Springer, New York, 2006, pp.205-235.

[46] N.K. Karmakar, S. Pandey, R.K. Pandey, S.S. Shukla, Solvatochromism: A tool for solvent discretion for UV-Vis spectroscopic studies. Appl. Spectrosc. Rev., 56 (2021), pp. 56:513-529.